Unraveling the Steric Link to Copper Precursor Decomposition: A Multi-Faceted Study for the Printing of Flexible Electronics

Shreya Mrig, Malavika A. Bhide, Ye Zhou, Nils Stanton, Jingyan Wang, Samuel P. Douglas, Henry R. Tinker, Kristian L. Mears, Clare M. Bakewell, and Caroline E. Knapp*

The field of printed electronics strives for lower processing temperatures to move toward flexible substrates that have vast potential: from wearable medical devices to animal tagging. Typically, ink formulations are optimized using mass screening and elimination of failures; as such, there are no comprehensive studies on the fundamental chemistry at play. Herein, findings which describe the steric link to decomposition profile: combining density functional theory, crystallography, thermal decomposition, mass spectrometry, and inkjet printing, are reported. Through the reaction of copper(II) formate with excess alkanolamines of varying steric bulk, tris-co-ordinated copper precursor ions: "[CuL$_3$]," each with a formate counter-ion (1–3) are isolated and their thermal decomposition mass spectrometry profiles are collected to assess their suitability for use in inks (I$^{1-3}$). Spin coating and inkjet printing of I^{1,2} provides an easily up-scalable method toward the deposition of highly conductive copper device interconnects ($\rho = 4.7$–5.3×10^{-7} Ω m; $\approx$30% bulk) onto paper and polyimide substrates and forms functioning circuits that can power light-emitting diodes. The connection among ligand bulk, coordination number, and improved decomposition profile supports fundamental understanding which will direct future design.

S. Mrig, Y. Zhou, N. Stanton, J. Wang, S. P. Douglas, H. R. Tinker,
K. L. Mears, C. E. Knapp
Department of Chemistry
University College London
20 Gordon Street, London WC1H 0AJ, UK
E-mail: caroline.knapp@ucl.ac.uk
M. A. Bhide, C. M. Bakewell
Department of Chemistry
King's College London
7 Trinity Street, London SE1 1DB, UK

The ORCID identification number(s) for the author(s) of this article can be found under https://doi.org/10.1002/smtd.202300038

1. Introduction

Economical, flexible, and compact electronic devices have become an important synthetic target as the market for printed electronics continues to expand.[1,2] Inkjet printing has emerged as an attractive alternative[3–6] to more conventional deposition methods. Metal-organic decomposition (MOD) inks that decompose at low temperatures are essential to capitalize on this printing technology.[7] Inks of this type generally incorporate a metal precursor, with the central metal ion coordinated to ligands that decompose to afford conductive metal upon post-deposition (e.g., thermal) treatment.[8] These inks have been heralded as an alternative to their traditional nanoparticle counterparts owing to the easy tunability of their ligands. Judicious ligand choice can allow for precursor decomposition at low (< 200 °C) temperatures.[9] This lower temperature processing has opened the field of printed electronics to low glass transition (T_g) flexible plastics and paper substrates.[10–12] As the third most conductive metal,[13] copper is an attractive choice for use in MOD precursors.[14] The criteria for the suitability of a MOD ink for inkjet printing include its ability to deposit coatings with conductivities comparable to that of the bulk metal at low temperatures (<200 °C), short sintering times, a long shelf life (>6 months), good substrate adhesion, and low environmental impact.[15]

There are several reports of MOD formulations that fulfil these criteria;[16–18] however, there is little evidence to explain how the ligands or additives used give rise to these desirable properties as well-defined, discrete compounds are rarely isolated. Earlier works present a multitude of thermal gravimetric analysis (TGA) profiles which show that changing the coordinating ligand to a central copper formate moiety can lead to a dramatic drop in decomposition temperature (up to 100 °C); however, no clear trends are highlighted.[19–21] Recently, hypothesized two-step decomposition mechanisms, via transient Cu(I) intermediates for copper(II) formate based precursors have been reported. TGA-mass spectrometry (MS) detected CO_2 as the first by-product leading to

**ADVANCED
SCIENCE NEWS**

www.advancedsciencenews.com

**small
methods**

www.small-methods.com

the conclusion that the two formate ligands are responsible for the reduction of the copper.[22–25] Marchal et al. used in situ X-ray absorption spectroscopy confirming the Cu(I) presence during reduction,[23] following this work with a study showing that bidentate ligands aided in oxidation prevention.[24]

A chemical explanation to this lowering effect upon coordination with alkanolamines remains unclear, highlighting the urgent need to ascertain the link between molecular structure and precursor properties[26] to make more informed decisions about ligand choice.[27–29]

There are few literature reports that attempt to establish this link[30] though Paquet et al.[31,32] have recently reported the isolation of a range of MOD complexes synthesized by the reaction of copper(II) formate with various pyridines and primary and secondary amines. This study suggested a link between increased H-bonding between the formate counter ion and the NH group of the ligand (confirmed by single crystal X-ray diffraction (SCXRD)) and rising decomposition temperatures from TGA. Paquet et al. have also reported TGA-MS consistent with results from Marchal, using electronic structure calculations to offer mechanistic insight into the decomposition profiles of copper(II) formate based precursors.[25] Ultimately however, the precursors reported did not form conductive copper upon decomposition.

Our group recently investigated the effect of steric demands of coordinating diamine/alkanolamines ligands on the decomposition temperature of copper(II) nitrate MOD precursors.[33] Using SCXRD, this work proposed that amine additives coordinated to the metal atom lengthened the copper–nitrate distance; thus, weakening the bond and lowering the decomposition temperature. These precursors could not convert thermally but did produce highly conductive ($\rho = 1.5 \pm 0.5 \times 10^{-6}$ Ω m) copper metal on glass when exposed to a reducing Ar/H$_2$ plasma.

2. Outline

Owing to the large number of derivatives, commercial availability, and potential for multiple coordination modes, we became interested in expanding the scope of these alkanolamine ligands with copper(II) formate, with the aim of isolating discrete complexes whose structure–reactivity relationship could be probed. 4-coordinate square planar complexes were synthesized by Bertrand and Muhonen[34,35] in the early 1980s from a hydrated copper source, but there is much scope for expansion both in terms of coordination number and ligand type. Herein, we explore the coordination of a series of alkanolamine ligands with copper(II) formate and for the first time, employ computational analysis to aid our understanding of the structural and observed decomposition profiles of the isolated complexes. This information aids our design of precursors for the printing of copper metal with high conductivity, suitable for electronic components from the synthesized inks.

3. Probing the Relationship Between Structure and Stability

3.1. Computational Studies

A series of copper complexes of the type [Cu(L)$_3$]$^+$[CHOO]$^-$ were targeted, where L corresponds to alkanolamines with increasing steric profile: 2-aminoethan-1-ol (L^1), 1-aminopropan-2-ol (L^2), and 2-amino-2-methylpropan-1-ol (L^3). These ligands have the ability to bind through both the N and O substituents, with 4-, 5-, and 6-coordinate complexes possible.[36,37] Therefore, we first used density functional theory (DFT) to gain an understanding of the geometries that might be expected from the different ligand combinations. A complex of the most simple alkanolamine, L^1, was modelled using a standard basis set (6-31G**/SDDAll) and a series of functionals (Table S1, Supporting Information).[38–40] In all cases, calculations consistently converged to complexes with either a 4- or 5- coordinate geometry around the central Cu atom, with attempts to model a complex where all three ligands were bound to the metal through both the O- and N- atoms unsuccessfully. A variety of additional O···H or N···H hydrogen bonding interactions were also observed, suggesting the ligand can provide additional stabilization to the complex (Table S1, Supporting Information). The formation of a 5-coordinate complex was found to be slightly less energetically favorable than the 4-coordinate complex ($\Delta G_{tetra–penta} = -3.27$ kcal mol^{-1}; wB97×, $\Delta G_{tetra–penta} = -0.64$ kcal mol^{-1}; M06L). These results indicate that complexes with a higher coordination number will be intrinsically less stable.

3.2. Synthesis

We next set about exploring these compounds experimentally, with dehydrated Cu(II) formate combined with an excess of L$^{1–3}$, which doubled as the reaction medium (**Scheme 1**). Compounds 1–3 were isolated as blue solids in high yields, with the [Cu(L)$_3$]$^+$[COOH]$^-$ composition confirmed by mass spectrometry (MS) and elemental analysis (EA). SCXRD was used to probe the finer bonding picture, with single crystals grown from saturated acetonitrile solution. FTIR (solid and solution) investigations of 1 and 2 showed only slight variation, indicating that structures reported in the SCXRD are representative of what is happening in solution. Compounds 1–3 were found to have drastically different solid state structures to each other, but in all cases, they contained a [Cu(L)$_3$]$^+$ fragment (**Figure 1**) with a single formate counter ion—in contrast to previously reported structures where two formate ligands are directly bound to the Cu ion.[24] The coordination number at copper reduced as the steric bulk of the ligand increased: 1 was hexacoordinate, 2 was pentacoordinate, and 3 was tetracoordinate; but in all cases, the formate was never bound to Cu^{2+}. In 1, all three ligands coordinated to the central copper ion in a bidentate fashion. As a result of steric constraints, O2 and O3 only weakly coordinated to the copper atom, as could be seen from their respective interatomic distances (Cu–O1: 1.9387(11) Å, Cu–O2: 2.4734(14) Å, and Cu–O3: 2.5297(15) Å). The Cu–O1 bond length was significantly shorter than that reported for a triflate analogue (Cu–O1: 1.960(2) Å),[36] which illustrates the importance of both ligand and counterion in these systems.

We therefore revisited the reaction of L^1 with [Cu(CHOO)$_2$(H$_2$O)$_4$] to investigate the coordination of L^1 in the presence of both co-ordinated formate and water molecules. When a 1:1 stoichiometry was used, no reaction occurred whilst 1:3 and greater would yield the previously reported CuL$_2$ compound.[34,35] Interestingly, a 1:2 stoichiometry yielded a tetrameric type-II cube-like copper alkoxide (4),[24,41] with the

ADVANCED
SCIENCE NEWS

www.advancedsciencenews.com

small
methods

www.small-methods.com
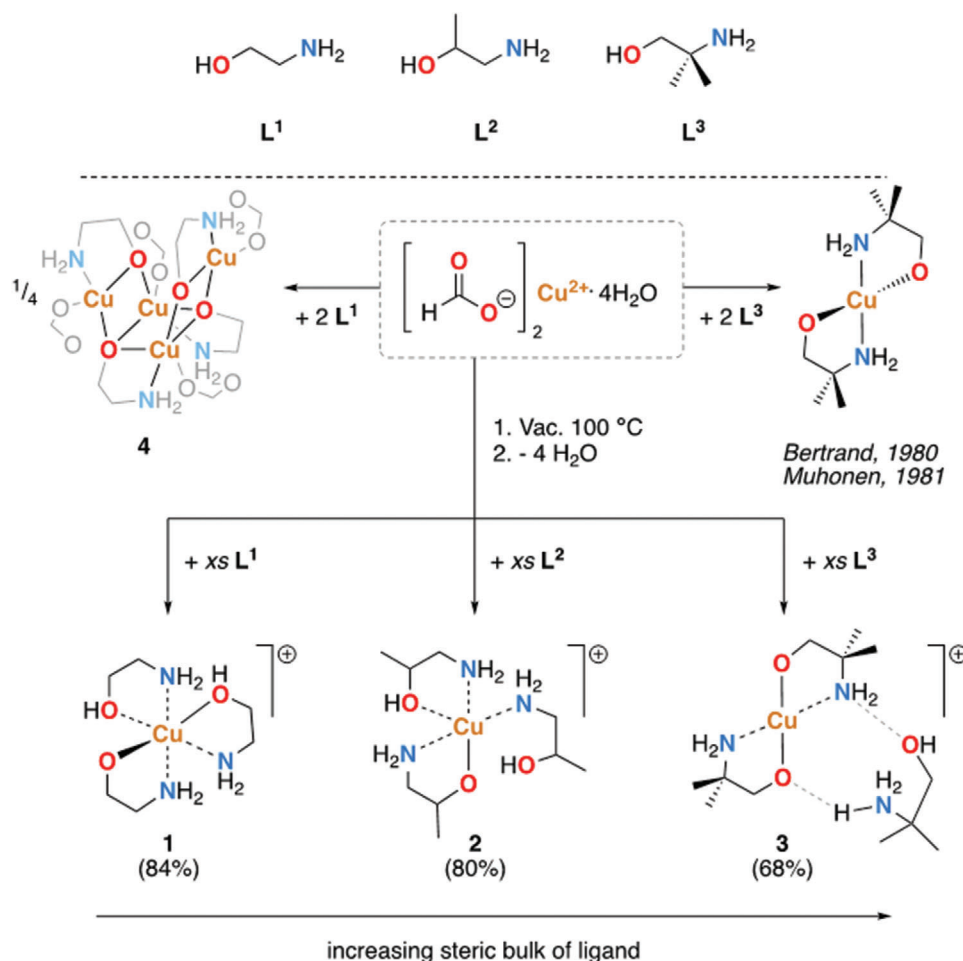
Scheme 1. Synthetic routes to compounds 1–4. Formate counter ions omitted for clarity, % yield given beneath.[34,35]
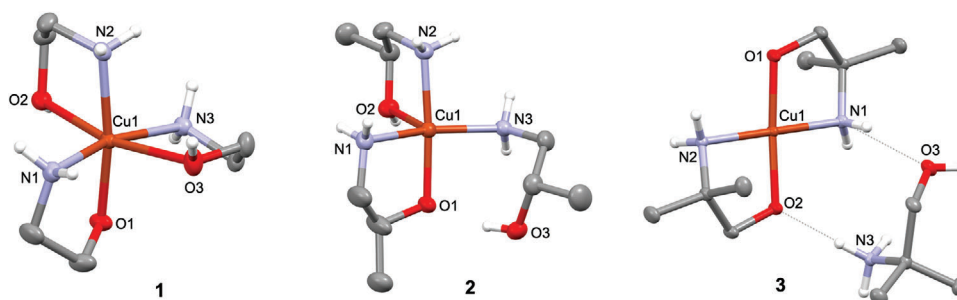
Figure 1. Molecular structures of 1 (left), 2 (middle), and 3 (right) with thermal ellipsoids drawn at 50% probability and selected hydrogen atoms and counter ions are omitted for clarity. In 3, grey dashed lines indicate hydrogen bonding.

formula $[Cu(CHOO)(L^1)]_4$ (Figure S1, Supporting Information). Here, each of the Cu atoms were coordinated by L^1 in a κ^2 fashion (e.g., Cu–O1: 1.9460(12) Å, Cu–N1: 2.010(13) Å) and a η^1-formate ligand (Cu–O2: 1.9613(12) Å). Bridging between Cu atoms occurs through the oxygen atoms of the alkanolamine such that each Cu is 4-coordinate.

In contrast to 1, due to the higher steric load on the carbon backbone of L^2, only two of the ligands display bidentate coordination in 2, while the third coordinates in a monodentate fashion

through N3. As in 1, compound 2 displays only one covalently bonded alkanolamine ligand through O1 (Cu–O1: 1.9908(7) Å), O2 datively coordinates (Cu–O2: 2.3087(13) Å) as do all the nitrogen atoms on the three ligands. The effect of the most sterically hindered ligand (L^3) results in the tetracoordinate compound 3, which unlike 1 and 2, has two covalently bound ligands (via O), resulting in shortened bond lengths of 1.901(2) Å (Cu–O1) and 1.910(2) Å (Cu–O2), both of which are significantly shorter than Bertrand's and Muhonen's complexes (which include a nitrate

counter-ion and water, respectively). A third L^3 N-cation is weakly coordinated to the O and N–H of the bound ligands through hydrogen bonding (Figure 1).

Thus, compound 1 showcases a [4 + 2] pseudo-octahedral arrangement around the copper atom in the solid state. This [4 + 2] coordination has been previously reported; however, axial sites are occupied either by counter ions[33] or molecules of hydration.[32] Compound 2 is 5-coordinate in the solid state, with $\tau_5 = 0.20$ ($\tau_5 = 0$ for square pyramid, $\tau_5 = 1$ for trigonal bipyramidal) corresponding to a slightly distorted square-based pyramidal geometry. Compound 3 showcases a square planar geometry $\tau_4 = 0.05$ ($\tau_4 = 0$ for square planar, $\tau_4 = 1$ for tetragonal), which is structurally similar to those previously reported.[34,35] The N–Cu–O internal bond angles at the copper atom are less than 90° because of the steric strain induced by the short backbone chain (O1–Cu–N1: 85.6(1)°; O2–Cu–N2: 85.5(1)°). τ values can give insight into the suitability of these compounds as precursors; higher distortion in precursors has previously been correlated with a reduction in decomposition temperature.[42] This would suggest that compound 2, with maximum distortion, would display the lowest decomposition temperature.

3.3. Thermal Decomposition

Following the isolation of compounds 1–4, their thermal decomposition behavior was investigated using thermal gravimetric analysis (TGA) in open pans with a N$_2$ shield gas to best reproduce real-world printing conditions. Following this, TGA-mass spectrometry (MS) was carried out on 1 and 2 and their corresponding inks (Figure S4, Supporting Information). Isolated compound 3 was found to be highly air sensitive and hygroscopic, with decomposition (Figure S2, Supporting Information) rendering the collection of TGA data impossible. For comparison, TGA data for commercially available hydrated copper formate and the in situ inks formulated from 1–3 in excess of their respective alkanolamine were also collected (**Figure 2**). All TGA profiles presented show a marked decrease in onset of decomposition temperature following complexing with the alkanolamine when compared to hydrated copper(II) formate alone (Figure 2, blue line).[27] The cluster compound, 4, did not fully decompose to copper metal (expected mass loss: 67.3%, actual: 45% at 168 °C) despite having a similar onset temperature to 1 and 2.

The decomposition products of 1 and 2 were found to be elemental copper (Figure S3, Supporting Information). Literature precedent for a two-step decomposition for copper formate inks with ethanolamine[22] is reproduced in this work as compound 1 degrades through a two-step thermal event which is initiated at ≈95 °C (taken from the point at which the data first deviates from dWt/dT = 0) and a second event at ≈195 °C, indicating that for complete conversion to copper metal, a minimum sintering temperature of 195 °C would need to be reached. Compound 2 appears to degrade through two thermal events which are initiated at ≈140 °C and ≈190 °C, indicating that deposition onto low-cost flexible materials could still be feasible, concurrent with our crystallographic findings that compound 2, with maximum distortion, would fully decompose at low temperature. TGA revealed that in situ inks saw a further reduction in onset of decomposition temperature, likely owing to the excess of alkanolamine
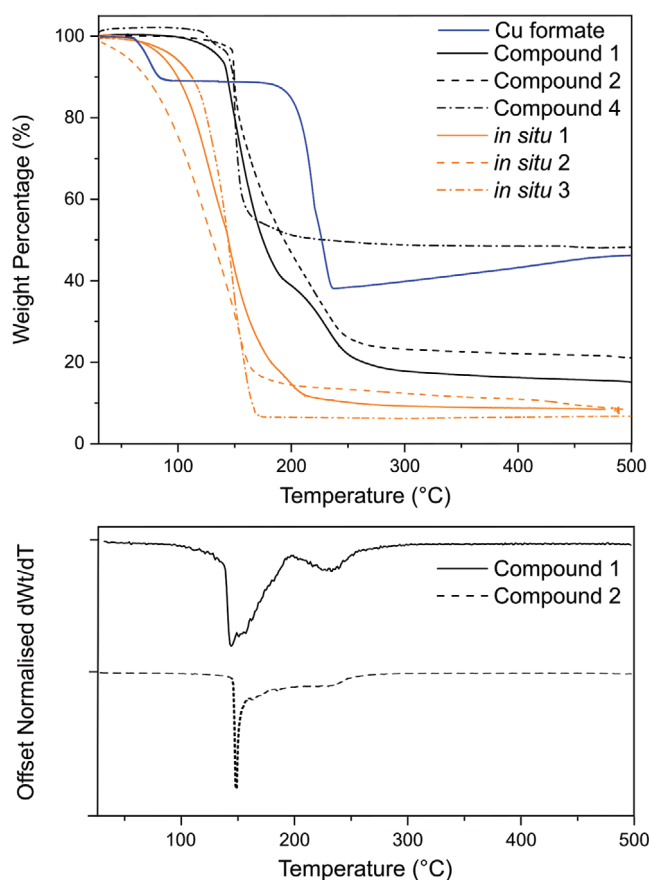

Figure 2. Top: overlapping thermograms for commercially available hydrated copper formate (blue), isolated compounds (black): 1 (solid), 2 (dash), and 4 (dot/dash), and in situ inks (orange) formulated from 1 (solid), 2 (dash), and 3 (dot/dash); Bottom: offset derivatives of thermograms for compounds 1 and 2.

present.[19] Whilst FTIR studies confirm the SCXRD structure of 1 and 2 to be representative of the solution based structures, TGA-MS was also carried out for solids (1, 2) and inks (I^1, I^2).

3.4. Printing Optimisation and Device Fabrication

The inks contain excess alkanolamines which can be detected in the TGA-MS as evaporating throughout the decomposition (for I^1 ethanolamine: m/z: 61; for I^2 1-aminopropan-2-ol: m/z: 75); it is also likely their incorporation aids in preventing oxidation consistent with previous literature findings.[24] A key finding from the TGA-MS of the isolated precursors, where no excess alkanolamines are present, is that decomposition products of both the formate counter-ion (CO$_2$: m/z 44) and fragments of the broken down alkanolamine (NH$_3$: m/z 17) are detected for both compounds 1 and 2. These data provide direct evidence that the alkanolamine ligand is involved in the reduction of the copper from +2 to 0. Previous DFT calculations had indicated that two copper bound formate ligands would be required to provide a sufficiently reducing environment for the complete conversion to metallic copper.[22–25] Boiling point of the alkanolamine has been previously demonstrated to alter the degradation profile of copper(II)

ADVANCED
SCIENCE NEWS
www.advancedsciencenews.com

small
methods
www.small-methods.com
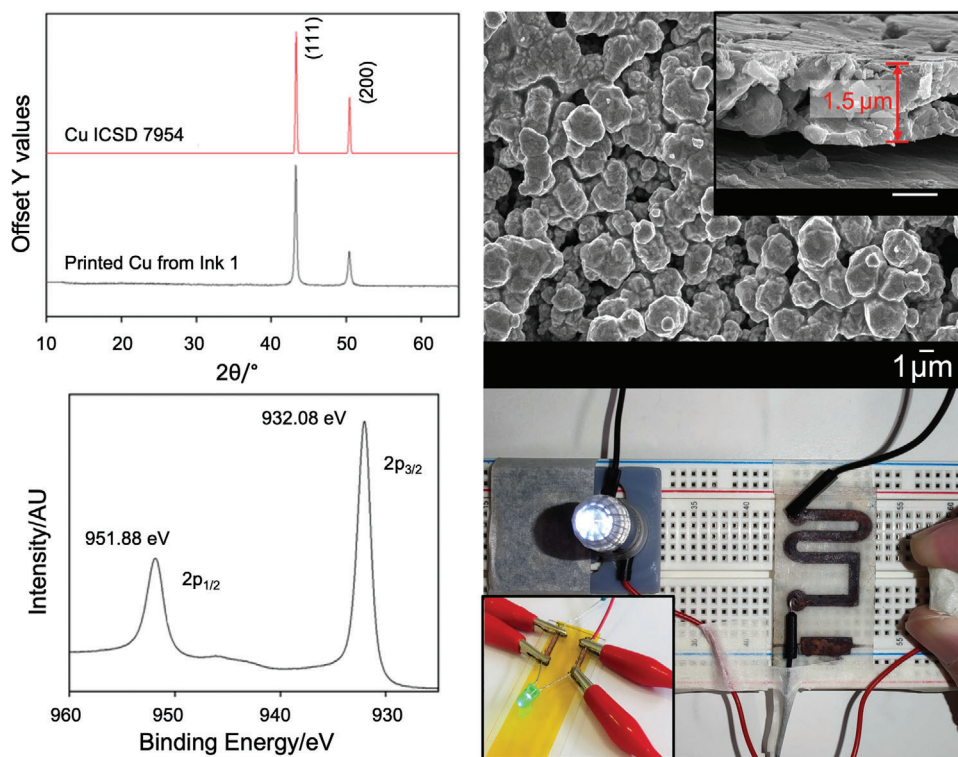
Figure 3. Properties of inkjet printed conductive Cu tracks. Top left: XRD pattern of printed Cu film, along with ICSD standard. Top right: SEM image of Cu on PI and (inset) cross-sectional SEM of Cu film on PI measuring 1.5 µm thickness. Bottom left: Cu 2p XPS of Cu film. Bottom right: Example of inkjet printed Cu on tracing paper (and inset on PI tape) used to light LEDs in circuits from I[1] and I[2], respectively.

formate based inks; in the TGA-MS, the lower boiling point additives (b.p. 1-aminopropan-2-ol: 150 °C) are released first, as expected, likely playing a role in the TGA profile of inks I[1–3].[27,32] Ultimately, it is likely that multiple decomposition pathways are possible; the in situ inks, which contain two equivalents of the formate counter-ion per copper ion in addition to excess alkanolamine would provide the best possible environment for reduction. Inclusion of formate counter ions in 1–3 as well as ligated alkanolamines facilitate the reduction of the Cu^{2+} ion upon heating, which certainly plays a part in lowering the energy requirements for this process.[27]

In situ inks I[1], I[2], and I[3] were then formulated for spin-coating and printing by mixing copper(II) formate with excess L[1], L[2], and L[3], respectively at room temperature (see Supporting Information). Initially, a proof-of-concept study was conducted to test the suitability of the inks as low temperature precursors toward elemental copper. Inks were drop cast or spin coated onto glass, paper, and polymers (e.g., polyimide (PI) and polyethylene terephthalate (PET)), followed by thermal sintering initially at 150 °C under an N_2 environment, which resulted in conductive copper deposits from all three inks on glass and polymers; repeats at 125 °C were also successful (Table S4, Supporting Information). This represents a reduction in processing temperature when compared to similar copper formate based inks with two equivalents of alkanolamines which required processing temperatures in the range of 140–250 °C.[22] This strengthens the hypothesis that ligand coordination number impacts the decomposition profile of the copper. Trial depositions onto paper were unsuccessful as the

drops of ink saturated the substrate. The deposits were characterized via XRD and X-ray photoelectron spectroscopy (XPS) which confirmed their identity as elemental copper, and scanning electron microscopy (SEM) revealed good coverage on all three substrates (Figures S4–S9, Supporting Information). While all three inks produced conductive copper, only I[1] and I[2] were selected to be inkjet printed.

The inkjet printing of two layers of I[1] onto glass and PI, followed by thermal sintering at 150 °C under an N_2 blanket resulted in highly conductive metallic copper ($\rho = 4.7$–5.3×10^{-7} Ω m) tracks. The printability of I[2] was improved by addition of ethanol which also facilitated superior wetting qualities onto paper substrates (Figure S11, Supporting Information). As such, I[2] in ethanol was inkjet printed onto paper and sintered at 150 °C under a blanket of N_2 producing conductive copper ($\rho = 3.83 \times 10^{-6}$ Ω m). In all cases, the tracks were relatively well adhered to the substrate, requiring physical abrasion with steel to cause delamination.

The X-ray diffraction patterns of the tracks deposited on glass, PI, and paper showed peaks indexed to the (111) and (200) planes of elemental copper. X-ray photoelectron spectra confirmed the presence of elemental copper, with peaks for the Cu $2p_{1/2}$ and Cu $2p_{3/2}$ states appearing at energies ≈ 951.0 eV and ≈ 932.00 eV, respectively for all samples, in agreement with literature values.[43] No peaks for copper(II) oxide were observed after a 300 s Ar-ion etch on any samples. Scanning electron microscopy (SEM) images showed a fully connected array of similar sized particulates coalesced together, consistent with the observed low resistivity.

Whilst the properties of copper patterns are highly related to their microstructure, the issue of pinholes in films can be easily remedied with a second pass on the printer; pinholes can be seen in the SEMs of single layer deposits, and these are unique to the use of molecular precursors as opposed to nanoparticle formulations, owing to the formation of gas during molecular precursor decomposition.[12]

Using these inkjet-printed copper interconnects as device electrodes, closed series circuits were built from a 9 V battery and a 5 mm dual in-line package LED (**Figure 3**; Figure S17, Supporting Information). This proof-of-concept experiment displayed the potential of these MOD precursors to develop electrical circuits on flexible materials at low temperatures.

4. Conclusion

In summary, ligand directed structural investigations have yielded a series of 4-, 5- and 6-coordinate copper MOD precursors (1–3). Whilst it may appear intuitive that the coordination number at copper will reduce as the steric bulk of the ligand increases, the fact that we have isolated a 6-coordinate Cu compound, which is counter-intuitive to our DFT predictions begins to build a picture as to why 1 acts as a superior ink additive.

The formation of these high-coordinate Cu complexes, which were confirmed by SCXRD studies, was facilitated by the use of a dehydrated copper(II) formate precursor. The strain of the molecules could be measured by the τ values obtained from crystallographic studies, which combined with DFT studies, indicates a decrease in complex stability with an increase in coordination number. Industrially, alkanolamine additives are routinely added to metal inks in trial-and-error experiments with no explanation given; however, we can confirm that the smaller the steric profile of the ligand, the higher the coordination geometry observed at the metal. Interestingly, crystallographic analysis revealed 2 to be most strained, which was a good fit with the superior TGA profile of the precursor, evidencing a subtle interplay between competing effects.

Ultimately the relative instability of the 5- and 6-coordinate complexes translated to their reactivity, with both compounds proving to be excellent MOD precursors. TGA-MS has shown both alkanolamine and formate ligands to be necessary for the complete reduction to metal in 1 and 2, with an excess of alkanolamines in the inks contributing to even lower decomposition temperatures. Compounds 1 and 2 have been shown from TGA and inkjet printing to be highly effective precursors to conductive metallic copper interconnects onto PI ($\rho = 4.7$–5.3×10^{-7} Ω m) and paper ($\rho = 3.83 \times 10^{-6}$ Ω m). This easily up-scalable method has yielded printed features a few microns thick, resulting in the realization of low-cost plastic or paper-based flexible electronics, demonstrated with an electrical circuit, which could have potential for use in high frequency devices which will be targeted in the lab for the next iteration.

For the first time, the combined analysis of complex structure, computational modelling, and reactivity studies has been applied to MOD precursors, unambiguously proving the complementary nature of these techniques. These investigations offer a more selective approach for the development of MOD precursors, and highlight the future importance of rational systems design.

Conflict of Interest

The authors declare no conflict of interest.

Data Availability Statement

The data that support the findings of this study are available from the corresponding author upon reasonable request.

[1] E. Dimitriou, N. Michailidis, *Nanotechnology* **2021**, *32*, 502009.
[2] S. P. Douglas, C. E. Knapp, *ACS Appl. Mater. Interfaces* **2020**, *12*, 26193.
[3] K. Fukuda, T. Someya, *Adv. Mater.* **2017**, *29*, 1602736.
[4] M. Vaseem, S.-K. Lee, J.-G. Kim, Y.-B. Hahn, *Chem. Eng. J.* **2016**, *306*, 796.
[5] M. Joo, B. Lee, S. Jeong, M. Lee, *Appl. Surf. Sci.* **2011**, *258*, 521.
[6] G. L. Draper, R. Dharmadasa, M. E. Staats, B. W. Lavery, T. Druffel, *ACS Appl. Mater. Interfaces* **2015**, *7*, 16478.
[7] D.-H. Shin, S. Woo, H. Yem, M. Cha, S. Cho, M. Kang, S. Jeong, Y. Kim, K. Kang, Y. Piao, *ACS Appl. Mater. Interfaces* **2014**, *6*, 3312.
[8] F. Hermerschmidt, D. Burmeister, G. Ligorio, S. M. Pozov, R. Ward, S. A. Choulis, E. J. W. List-Kratochvil, *Adv. Mater.* **2018**, *3*, 1800146.
[9] Y. Choi, K. Seong, Y. Piao, *Adv. Mater. Interfaces* **2019**, *6*, 1901002.
[10] S. Glatzel, Z. Schnepp, C. Giordano, *Angew. Chem., Int. Ed.* **2013**, *52*, 2355.
[11] D. Tobjörk, R. Österbacka, *Adv. Mater.* **2011**, *23*, 1935.
[12] C. E. Knapp, J.-B. Chemin, S. P. Douglas, D. A. Ondo, J. Guillot, P. Choquet, N. D. Boscher, *Adv Mater* **2018**, *3*, 1700326.
[13] *CRC Handbook of Chemistry and Physics: A Ready-Reference Book of Chemical and Physical Data* (Eds: W. M. Haynes and D. R. Lide), CRC Press, Boca Raton, FL **2015**.
[14] S. M. Song, S. M. Cho, *ACS Appl. Electron. Mater.* **2022**, *4*, 1882.
[15] S. P. Douglas, S. Mrig, C. E. Knapp, *Chemistry* **2021**, *27*, 8062.
[16] H. M. Lee, S.-Y. Choi, K. T. Kim, J.-Y. Yun, D. S. Jung, S. B. Park, J. Park, *Adv. Mater.* **2011**, *23*, 5524.
[17] S. B. Walker, J. A. Lewis, *J. Am. Chem. Soc.* **2012**, *134*, 1419.
[18] B. Deore, C. Paquet, A. J. Kell, T. Lacelle, X. Liu, O. Mozenson, G. Lopinski, G. Brzezina, C. Guo, S. Lafrenière, P. R. L. Malenfant, *ACS Appl. Mater. Interfaces* **2019**, *11*, 38880.

[19] A. Yabuki, S. Kawahara, S. Kang, I. W. Fathona, *Mater. Sci. Eng., B* **2020**, *262*, 114743.

[20] A. Yabuki, S. Tanaka, *Mater. Res. Bull.* **2012**, *47*, 4107.

[21] A. Yabuki, N. Arriffin, M. Yanase, *Thin Solid Films* **2011**, *519*, 6530.

[22] Y. Farraj, M. Grouchko, S. Magdassi, *Chem. Commun.* **2015**, *51*, 1587.

[23] W. Marchal, A. Longo, V. Briois, K. Van Hecke, K. Elen, M. K. Van Bael, A. Hardy, *Inorg. Chem.* **2018**, *57*, 15205.

[24] W. Marchal, F. Mattelaer, K. Van Hecke, V. Briois, A. Longo, D. Reenaers, K. Elen, C. Detavernier, W. Deferme, M. K. Van Bael, A. Hardy, *Langmuir* **2019**, *35*, 16101.

[25] H. Shin, X. Liu, T. Lacelle, R. J. MacDonell, M. S. Schuurman, P. R. L. Malenfant, C. Paquet, *ACS Appl. Mater. Interfaces* **2020**, *12*, 33039.

[26] J. A. Manzi, C. E. Knapp, I. P. Parkin, C. J. Carmalt, *Eur. J. Inorg. Chem.* **2015**, *2015*, 3658.

[27] A. Yabuki, Y. Tachibana, I. W. Fathona, *Mater. Chem. Phys.* **2014**, *148*, 299.

[28] M. T. Ackermann, M. Seidl, F. Wen, M. J. Ferguson, A. Y. Timoshkin, E. Rivard, M. Scheer, *Chem. – Eur. J.* **2022**, *28*, e202103780.

[29] K. L. Mears, C. R. Stennett, E. K. Taskinen, C. E. Knapp, C. J. Carmalt, H. M. Tuononen, P. P. Power, *J. Am. Chem. Soc.* **2020**, *142*, 19874.

[30] M. A. Bhide, K. L. Mears, C. J. Carmalt, C. E. Knapp, *Chem. Sci.* **2021**, *12*, 8822.

[31] C. Paquet, T. Lacelle, B. Deore, A. J. Kell, X. Liu, I. Korobkov, P. R. L. Malenfant, *Chem. Commun.* **2016**, *52*, 2605.

[32] C. Paquet, T. Lacelle, X. Liu, B. Deore, A. J. Kell, S. Lafrenière, P. R. L. Malenfant, *Nanoscale* **2018**, *10*, 6911.

[33] C. E. Knapp, E. A. Metcalf, S. Mrig, C. Sanchez-Perez, S. P. Douglas, P. Choquet, N. D. Boscher, *ChemistryOpen* **2018**, *7*, 850.

[34] J. A. Bertrand, E. Fujita, D. G. VanDerveer, *Inorg. Chem.* **1980**, *19*, 2022.

[35] H. Muhonen, *Acta Crystallogr., Sect. B: Struct. Crystallogr. Cryst. Chem.* **1981**, *37*, 951.

[36] H. D. Pratt, J. C. Leonard, L. A. M. Steele, C. L. Staiger, T. M. Anderson, *Inorg. Chim. Acta* **2013**, *396*, 78.

[37] N. Podjed, B. Modec, R. Clérac, M. Rouzières, M. M. Alcaide, J. López-Serrano, *New J. Chem.* **2022**, *46*, 6899.

[38] W. J. Hehre, R. Ditchfield, J. A. Pople, *J. Chem. Phys.* **1972**, *56*, 2257.

[39] P. C. Hariharan, J. A. Pople, *Theor. Chim. Acta* **1973**, *28*, 213.

[40] T. Clark, J. Chandrasekhar, G. W. Spitznagel, P. V. R. Schleyer, *J. Comput. Chem.* **1983**, *4*, 294.

[41] R. Mergehenn, W. Haase, *Acta Crystallogr., Sect. B: Struct. Sci., Cryst. Eng. Mater.* **1977**, *33*, 1877.

[42] M. A. Bhide, K. L. Mears, C. J. Carmalt, C. E. Knapp, in *Nanomaterials Via Single-Source Precursors*, 1st ed. (Eds.: A.W. Apblett, A.R. Barron, A.F. Hepp), Elsevier, Amsterdam, the Netherlands **2022**, pp. 3–53.

[43] A. C. Miller, G. W. Simmons, *Surf. Sci. Spectra* **1993**, *2*, 55.